Tubular PFKFB3 drives diabetic kidney fibrosis via lactate-dependent H4K12 lactylation and HIPK2 transactivation

MINGKUN XU[1*], LINHANG FU[2*], YULONG ZHANG[2], XIULI GUO[3], HAN WU[3], SIJING GAO[4], FEI XIAO[5] and LI XU[3]

[1]Department of Anesthesiology, Affiliated Hospital of Guangdong Medical University, Zhanjiang, Guangdong 524003, P.R. China; [2]Department of Anesthesiology, The Second Affiliated Hospital of Guangdong Medical University, Zhanjiang, Guangdong 524003, P.R. China; [3]Department of Laboratory Medicine, The Second Affiliated Hospital of Guangdong Medical University, Zhanjiang, Guangdong 524003, P.R. China; [4]International Medical and Special Care Ward, The Affiliated Hospital of Guangdong Medical University, Zhanjiang, Guangdong 524002, P.R. China; [5]Department of Laboratory Medicine, Maoming People's Hospital, Maoming, Guangdong 525099, P.R. China

Received November 27, 2025; Accepted June 3, 2026

DOI: 10.3892/ijmm.2026.5926

Abstract. Aerobic glycolysis is increasingly recognized as a pathogenic driver in diabetic kidney disease (DKD). However, the epigenetic role of its end product, lactate, remains largely undefined. Spatial transcriptomics analysis revealed active glycolysis in tubular epithelial cells. The participation of histone lactylation in DKD was confirmed through inhibition of histone lactylation by glycolysis inhibitors or lactate in vivo. The potential target genes of H4K12 lactylation (H4K12la) were screened by CUT&Tag analyses. The candidate target genes were validated through ChIP-qPCR, RT-qPCR and western blot analyses. The present study found that the expression of 6-phosphofructo-2-kinase/fructose-2,6-biphosphatase 3 (PFKFB3), a pivotal glycolytic regulator, was markedly upregulated in tubular epithelial cells derived from patients with DKD and from the corresponding mouse models. Inhibition of the expression of PFKFB3 mitigated the kidney fibrotic process and alleviated renal function in a DKD mouse model. Conversely, upregulation of PFKFB3 expression aggravated renal fibrogenesis and promoted the deterioration of renal pathology. Moreover, it was demonstrated that the reduction in the levels of lactate levels markedly alleviated renal fibrosis in DKD. With regard to its mechanism of action, lactate was generated via PFKFB3-driven glycolytic reprogramming and selectively enhanced H4K12 lactylation at the homeodomain-interacting protein kinase 2 (HIPK2) promoter, thereby activating its transcription and driving renal fibrotic progression. These findings indicated that PFKFB3 in renal tubules upregulates HIPK2 expression via facilitating H4K12la-dependent gene transcription. Therefore, intervention approaches targeting PFKFB3-triggered HIPK2 activation in tubular cells may offer a novel therapeutic strategy for DKD.

Correspondence to: Dr Li Xu, Department of Laboratory Medicine, The Second Affiliated Hospital of Guangdong Medical University, 12 Wenming East Road, Xiashan, Zhanjiang, Guangdong 524003, P.R. China
E-mail: xulicmu@163.com

Dr Fei Xiao, Department of Laboratory Medicine, Maoming People's Hospital, 101 Weimin Road, Maoming, Guangdong 525099, P.R. China
E-mail: xiaofei536@126.com

*Contributed equally

Key words: diabetic kidney disease, tubular epithelial cells, 6-phosphofructo-2-kinase/fructose-2,6-biphosphatase 3, Histone H4, Lysine 12 lactylation

Introduction

Diabetes mellitus has emerged as the predominant cause of chronic kidney disease worldwide. Up to 40% of diabetic patients progress to renal dysfunction, with the burden of type 2 diabetes-related chronic kidney disease increasing substantially in recent decades (1). Diabetic kidney disease (DKD), a severe microvascular complication of diabetes, constitutes the main contributor to end-stage renal disease (ESRD) and imposes a substantial clinical and socioeconomic burden (2,3). Since DKD progresses to renal failure, healthcare costs and patient mortality rise markedly, while effective therapeutic options for DKD remain limited (4,5). Consequently, elucidating the mechanism driving DKD progression and identifying potential therapeutic targets are necessary.

Hyperglycemia triggers molecular perturbations that amplify oxidative stress and promote the production of inflammatory cytokines, growth factors, and profibrotic mediators (6,7). These molecular pathway ultimately lead to renal fibrosis, a major determinant of DKD progression to ESRD (8,9). During renal fibrosis, tubular epithelial cells (TECs) are lost via various forms of cell death, while surviving cells undergo dedifferentiation, characterized by downregulation of epithelial markers and upregulation of

mesenchymal markers (10,11). Defective tubular repair and regeneration are now recognized as pivotal contributors to persistent renal inflammation and fibrotic remodeling (12-14). However, the molecular mechanisms responsible for TEC injury and subsequent fibrotic progression remain incompletely understood.

TECs represent the structural and functional core of renal tubules and are responsible for reabsorbing essential solutes, a process that demands considerable energy consumption (15). Tubular reabsorption is an energy-intensive process and, owing to their high mitochondrial content, TECs exhibit higher sensitivity to hypoxic conditions than other renal cell types (16,17). Under physiological conditions, TECs preferentially rely on fatty acid oxidation (FAO) to generate ATP efficiently (18,19). Under pathological conditions, inhibition of the FAO pathway in TEC triggers a metabolic transition toward glycolysis (19). Although this adaptive glycolytic response can temporarily mitigate energy imbalance, sustained glycolysis drives excessive accumulation of intermediates such as lactate, ultimately aggravating TECs injury (20). Concomitantly, suppression of FAO results in lipid droplet deposition and activates inflammatory signaling pathways, mitochondrial dysfunction and epithelial-mesenchymal transition (EMT), collectively driving the progression of tubulointerstitial fibrosis (18,21,22). Therefore, restoring balanced metabolic flux in TECs may represent a promising strategy for preserving renal function.

Lactate, a key product of glycolysis, plays dual roles in metabolism and cellular signaling. In patients with type 1 diabetes, strong correlations have been observed between glucose and lactate concentrations in plasma and urine (23). Accumulating evidence indicates that glycolysis induced lactate production partially originates from TECs, as inhibition of the sodium-glucose cotransporter-2 (SGLT2) markedly reduces lactate generation in kidney tissues and in SGLT2-deficient mice (23). Beyond its metabolic role, lactate functions as a precursor for histone lactylation, a newly discovered epigenetic modification implicated in the modulation of gene transcription (24,25). Research demonstrates that increased lactate levels drive H3K14la modification, thereby promoting EMT and contributing to renal tubular fibrosis in DKD (26). Nevertheless, the overall function of histone lactylation during the pathogenesis of DKD has not been fully elucidated.

Collectively, these results indicate that DKD enhances 6-phosphofructo-2-kinase/fructose-2,6-biphosphatase (PFKFB) 3 expression and triggers homeodomain-interacting protein kinase 2 (HIPK2) lactylation at H4K12, uncovering a previously unrecognized mechanism and a potential target for the prevention of renal dysfunction in DKD.

Materials and methods

Human specimens. A total of 60 patients were enrolled in this study, with a male-to-female ratio of 2:3. The participants ranged in age from 18-65 years. Patient recruitment was conducted between March 2024 and March 2025. Renal biopsy specimens from patients with DKD were collected from the Department of Nephrology at the Second Affiliated Hospital of Guangdong Medical University using needle biopsy. Normal control renal tissues were obtained from histologically normal, non-tumorous regions of nephrectomy specimens via wedge biopsy, located at least 5 cm away from the tumor margin and were confirmed intraoperatively by pathological examination to be free of malignant cell infiltration (27). Written informed consent was obtained from all patients. All procedures were approved by the Medical Ethics Committee of the Second Affiliated Hospital of Guangdong Medical University (approval no. YSC202400101, 2024) and were performed in accordance with the Declaration of Helsinki.

Animal models and experimental design. Male BKS. Cg-Dock7m$^{+/+}$ Leprdb/J (db/db) mice, together with their age-matched non-diabetic lean db/m littermates, were purchased from the Model Animal Research Center of Nanjing University. A total of 100 male mice (db/m weighting 27±5 g, db/db weighting 41±10 g), were raised to 10 weeks old housed under specific pathogen-free (SPF) conditions at a constant temperature of (23±2˚C), relative humidity of 50-60%, with a 12-h light/dark cycle. Animals had free access to standard chow and sterile acidified drinking water *ad libitum*. Experimental protocols were approved by the Animal Ethics Committee of Guangdong Medical University (approval no. GDY2402166, 2024). Mice in the treatment groups were administered FX-11 at a dose of 15 mg/kg via intraperitoneal injection once daily for 10 weeks.

For PFKFB3 knockdown, an adeno-associated virus (AAV9) encoding a short hairpin RNA targeting PFKFB3 (shPFKFB3 target sequence: GCCTCCAACATCATGGAAGTT; shNC target sequence: 5'-CCTAAGGTTAAGTCGCCCTCG-3', Shanghai GeneChem Co., Ltd.) was injected directly into the renal pelvis of db/db mice at 10 weeks of age.

Biochemical analyses. Blood glucose concentrations were measured using a Roche Diabetes Care glucometer (Roche Diagnostics, Ltd.) from tail vein blood samples collected at 8 weeks of age. Mice exhibiting a fasting blood glucose level exceeding 16.7 mM were considered successfully diabetic. Urinary albumin, urinary creatinine, and serum creatinine levels were quantified using commercial kits from Roche Diagnostics, Ltd., following previously established protocols (28). Starting from 10 weeks of age, the db/db group received AAV-shPFKFB3 treatment and all groups were fasted for at least 8 h prior to blood glucose and urine tests, during which free access to water was permitted. Anesthesia was induced in an induction chamber with 5% isoflurane delivered in 100% oxygen at a flow rate of 1.5 l/min, and was continued until the loss of righting and pedal reflexes was confirmed. A blood volume of ~1.43 ml was obtained from each mouse via cardiac puncture at 20 weeks of age.

Animal sacrifice. According to the AVMA Guidelines for the Euthanasia of Animals (2020 Edition) (29), at the end of the experimental protocol, all animals were humanely sacrificed. In accordance with the approved animal ethics protocol, mice were euthanized by overdose of isoflurane anesthesia. Briefly, mice were placed in an induction chamber and exposed to 5% isoflurane in oxygen until deep anesthesia was achieved, as confirmed by the absence of pedal withdrawal and corneal reflexes. Isoflurane exposure was continued for at least 1 min after respiratory arrest. Mortality was further confirmed by

the absence of respiration, heartbeat and reflex responses, followed by vital organ harvest.

Cell culture and in vitro treatments. Human proximal tubular epithelial (HK-2) cells were cultured in DMEM/F12 medium supplemented with 10% fetal bovine serum. To model diabetic conditions, cells were exposed to high glucose (HG; 30 mM), with normal glucose (NG; 5.5 mM) as control. PFKFB3 silencing was achieved by transfecting HK-2 cells with small interfering (si)RNA targeting PFKFB3 (siPFKFB3) at a final concentration of 50 nM using Lipofectamine® RNAiMAX Transfection Reagent (Thermo Fisher Scientific, Inc.) according to the manufacturer's instructions. Cells were incubated with the transfection complex at 37˚C for 6 h, after which the medium was replaced with fresh complete medium. Cells were harvested for subsequent experiments 48 h after transfection. The siNC (5'-UUCUCCGAACGUGUCACGUTT-3') was used as a normal control. For lactate supplementation experiments, cells were treated with 10 mM sodium L-lactate (cat. no. S108838, Aladdin) in addition to HG conditions.

Spatial transcriptomics analysis of DKD patient samples. The spatial transcriptomics (ST) data of human DKD kidney samples have been deposited in the Gene Expression Omnibus (GEO) database at the National Center for Biotechnology Information (accession number: GSE261545; https://www.ncbi.nlm.nih.gov/geo/query/acc.cgi?acc=GSE261545). For the present study, the ST datasets were retrieved from this GEO repository (https://www.ncbi.nlm.nih.gov/geo/). Dimensionality reduction was conducted using the Seurat package (version 4.2.2; https://satijalab.org/seurat/) within the R software environment (version 4.3.2; https://cran.r-project.org/bin/windows/base/old/4.3.2/). Previously established morphology-based clustering annotations were incorporated into the metadata. SCTransform was applied for data normalization and scaling using Seurat (version 4.2.2) in the R environment (version 4.3.2). The first 20 principal components were then used for Uniform Manifold Approximation and Projection to achieve dimensionality reduction, generating a comparable number of clusters for assessment against the morphology-based clusters. Subsequently, high-resolution spatial plots were generated to visualize the spatial distribution of these clusters alongside the expression levels of feature genes. The Loupe file produced by the 10X Space Ranger pipeline (10x Genomics; https://www.10xgenomics.com) was initially opened in the Loupe Browser (10x Genomics; version 6.5.0; https://www.10xgenomics.com/products/loupe-browser). A renal pathologist (P.I.) used hematoxylin and eosin (H&E)-stained (hematoxylin, 5 min; eosin, 2 min at room temperature) bright-field mosaics (ST slide) as anatomical references to perform morphology-based clustering for each spatially resolved spot on the Visium slide (Wuhan Servicebio Technology Co., Ltd.). This process involved manual delineation of renal morphological structures and lesions to identify the clusters.

Gene Ontology (GO) enrichment analysis. GO enrichment analysis was performed using the clusterProfiler R package (version 4.3.2; https://bioconductor.org/packages/release/bioc/html/clusterProfiler.html) based on the GO database. Differentially expressed genes were subjected to enrichment analysis, and terms with $P<0.05$ and FDR <0.05 were considered significantly enriched. Results were visualized using R software.

Histological assessment and immunohistochemistry (IHC). Kidney tissues were fixed in 10% neutral-buffered formalin at room temperature for 24 h, dehydrated through a graded ethanol series, cleared in xylene, and embedded in paraffin. Paraffin-embedded tissues were sectioned at 3 μm. For Masson's trichrome staining, sections were stained using a Masson's Trichrome Staining kit (Wuhan Servicebio Technology Co., Ltd.) at room temperature for 10 min according to the manufacturer's instructions. For Sirius Red staining, sections were stained using a Picro Sirius Red Staining kit (Wuhan Servicebio Technology Co., Ltd.) at room temperature for 60 min. For immunohistochemistry, sections were deparaffinized and rehydrated, followed by permeabilization with 0.1% Triton X-100 for 10 min. Endogenous peroxidase activity was quenched with 3% hydrogen peroxide for 10 min. Sections were blocked with 5% bovine serum albumin (BSA) at room temperature for 30 min. Sections were incubated overnight at 4˚C with primary antibodies against PFKFB3 (Proteintech Group, Inc.; cat. no. 13763-1-AP. 1:100), fibronectin (Abcam; cat. no. ab2413, 1:200), or α-smooth muscle actin (α-SMA; Abcam; cat. no. ab5694, 1:200). After washing, sections were incubated with appropriate horseradish peroxidase-conjugated secondary antibodies (1:500; Wuhan Servicebio Technology Co., Ltd.) at room temperature for 1 h. Immunoreactivity was visualized using diaminobenzidine (DAB), followed by hematoxylin counterstaining for 3 min at room temperature. Images were acquired using a light microscope at x200 and x400 magnification.

Lactate quantification. Lactate levels in kidney tissue homogenates and HK-2 cell culture supernatants were measured using a colorimetric assay kit (Biovision; Abcam Bio X Cell; cat. no. K627-100) according to the manufacturer's protocol. Absorbance was read at 450 nm using a microplate reader, and lactate concentrations were calculated from a standard curve.

Immunofluorescence (IF). For immunofluorescence staining, frozen kidney sections (3 μm) or cultured HK-2 cells were fixed in ice-cold methanol/acetone for 10 min and washed with phosphate-buffered saline (PBS). Samples were blocked with 5 % BSA (Beyotime Biotechnology; cat. no. ST027) in PBS for 1 h at room temperature. Cells or sections were then incubated overnight at 4˚C with primary antibodies against E-cadherin (Santa Cruz Biotechnology, Inc.; cat. no. sc-59778), PFKFB3 (Abcam, ab181861), H4K12la (PTM Bio, PTM-1411RM,), or HIPK2 (Abcam; cat. no. ab108543), all the primary antibody were diluted to 1:500. After washing with PBS, samples were incubated with fluorophore-conjugated secondary antibodies (1:1,000; Invitrogen; Thermo Fisher Scientific, Inc.) for 1 h at room temperature in the dark. Nuclei were counterstained with DAPI (1 μg/ml) for 5 min at room temperature. Fluorescence images were captured using a fluorescence microscope.

Western blotting. Total proteins were extracted from mice kidney tissues and HK-2 cells using RIPA lysis buffer containing protease and phosphatase inhibitors (Beyotime Biotechnology; cat. no. P0013B,). Protein concentrations were determined using a BCA Protein Assay Kit (Beyotime Biotechnology; cat. no. P0010). Equal amounts of protein (20 μg per lane) were separated by 10% SDS-polyacrylamide gel electrophoresis and transferred onto polyvinylidene difluoride membranes. Following 1 h blocking with 5% non-fat milk at 25˚C and the membranes incubated overnight at 4˚C with primary antibodies against PFKFB3 (1:1,000; Abcam; cat. no. ab181861,), fibronectin (1:1,000; Abcam ab2413,), α-SMA (1:1,000; Abcam; cat. no. ab5694,), H4K12la (1:1,000; PTMBio, PTM-1411RM), HIPK2 (1:1,000; Abcam; cat. no. ab108543,), or β-actin (1:10,000, loading control; Abcam; cat. no. ab8226,) for 1 h at room temperature. After incubation with horseradish peroxidase-conjugated secondary antibodies (1:10,000; Novus Biologicals; Bio-Techne), protein bands were visualized using an Enhanced Chemiluminescence (ECL) Detection Kit (Beyotime Biotechnology; cat. no. P0018FS) and quantified using Image J (version 1.52a; National Institutes of Health).

RNA extraction and reverse transcription-quantitative (RT-q) PCR. HK-2 cells were seeded at a density of $3x10^5$ cells/well in 6-well plates and harvested for RNA extraction. Total RNA was isolated from HK-2 cells and mice kidney tissues using TRIzol® reagent (Invitrogen; Thermo Fisher Scientific, Inc.) according to the manufacturer's instructions. RNA concentration and purity were determined using a Nanodrop spectrophotometer. Reverse transcription was performed using a PrimeScript RT Reagent Kit (Takara Bio, Inc.) according to the manufacturer's protocol. Quantitative PCR was carried out using TB Green Premix Ex Taq II (Takara Bio, Inc.) on a LightCycler Real-Time PCR System (Roche Diagnostics Ltd.) according to the manufacturer's instructions. The PCR cycling conditions were as follows: Initial denaturation at 95˚C for 30 sec, followed by 40 cycles of denaturation at 95˚C for 5 sec and annealing/extension at 60˚C for 30 sec. Gene expression levels were normalized to β-actin as an internal control, and relative fold changes were calculated using the $2^{-\Delta\Delta Cq}$ method (30). Primer sequences are provided in Table SI. All experiments were performed in triplicate and repeated at least three independent times.

CUT&Tag sequencing. HK-2 cells ($1x10^5$ cells per sample) were harvested and subjected to CUT&Tag assay using the Hyperactive CUT&Tag-seq kit (Vazyme Biotech Co., Ltd.; cat. no. 904). Briefly, cells were bound to concanavalin A-coated magnetic beads, followed by sequential incubation with anti-H4K12la antibody (PTMBio; cat. no. PTM-1411RM), a secondary antibody (goat anti-rabbit IgG H&L) (Abcam), and a hyperactive pA/G-TN5 transposase (Vazyme Biotech Co., Ltd.). Tagmented DNA fragments were extracted, amplified by PCR, and purified for library preparation. Library quality was assessed using a LabChip system, and sequencing was performed on an Illumina platform. The raw and processed sequencing data have been uploaded to the NCBI GEO database under accession number GSE328635 (https://www.ncbi.nlm.nih.gov/geo/query/acc.cgi?acc=GSE328635).

Chromatin immunoprecipitation (ChIP)-qPCR. ChIP assays were performed using a commercial Chromatin Immunoprecipitation Kit (MilliporeSigma; cat. no. 17-371). HK-2 cells were seeded at a density of $2x10^6$ cells per 10 cm dish and cultured prior to experiments. Immunoprecipitation was carried out overnight at 4˚C using either an anti-H4K12la antibody (1:100; PTMBio; cat. no. PTM-1411) or normal rabbit IgG as a negative control with 25-50 μg of sheared chromatin per immunoprecipitation reaction and 2-5 μg antibody per IP. A 1-5% aliquot of chromatin was saved as Input prior to immunoprecipitation. After reversing cross-links and purifying DNA, enrichment of specific genomic regions was analyzed by qPCR using promoter-specific primers (Table SII). PCR amplification was carried out using DreamTaq DNA polymerase (Thermo Fisher Scientific, Inc.; cat. no. 10342020). The cycling program was: 95˚C for 3 min; 35 cycles of 95˚C for 30 sec, 58˚C for 30 sec, 72˚C for 30 sec; and 72˚C for 5 min. PCR products were electrophoresed on a 1.5% agarose gel, stained with ethidium bromide, and imaged using a ChemiDoc MP system (Bio-Rad Laboratories, Inc.). Washing steps were performed using the buffers provided in the kit, including low-salt, high-salt, LiCl, and TE wash buffers. Results are presented as percentage of input relative to IgG control. Quantification was performed using the Applied Biosystems 7500 Real-Time PCR System (Thermo Fisher Scientific, Inc.) and SDS software (v2.4; (Applied Biosystems; Thermo Fisher Scientific, Inc.).

Glycolytic flux measurement. Extracellular acidification rate (ECAR), a proxy for glycolytic activity, was measured using a Seahorse XF^{96} extracellular flux analyzer (Agilent Technologies, Inc.). HK-2 cells were seeded into XF^{24} V7 cell culture microplates and incubated for 2 h at 37˚C in assay medium containing 10 mM glucose. Subsequently, oligomycin (an ATP synthase inhibitor) and 2-deoxyglucose (a glycolysis inhibitor) were sequentially injected, and ECAR was recorded at regular intervals to assess basal glycolysis, glycolytic capacity, and glycolytic reserve.

Statistical analysis. Data represent mean ± SD from three independent replicates. Statistical evaluation was carried out using SPSS 15.0 (SPSS, Inc.). Unpaired two-tailed t-tests were applied for pairwise comparisons, and one-way ANOVA with Bonferroni correction was used for multiple groups. $P<0.05$ was considered to indicate a statistically significant difference.

Results

Elevated expression of PFKFB3 is associated with renal proximal tubules injury in DKD. ST profiling was performed on H&E-stained renal sections from patients with DKD to visualize transcriptional landscapes within histological context. ST analysis identified a series of spatial 'spots' that were mapped onto the renal microanatomy, encompassing glomeruli, tubules, vascular regions and tubular casts. Reanalysis of a publicly available ST data enabled improved mapping resolution and the identification of rare cell populations contributing to local transcriptomic heterogeneity (Fig. 1A). Distinct clusters emerged, each displaying marked

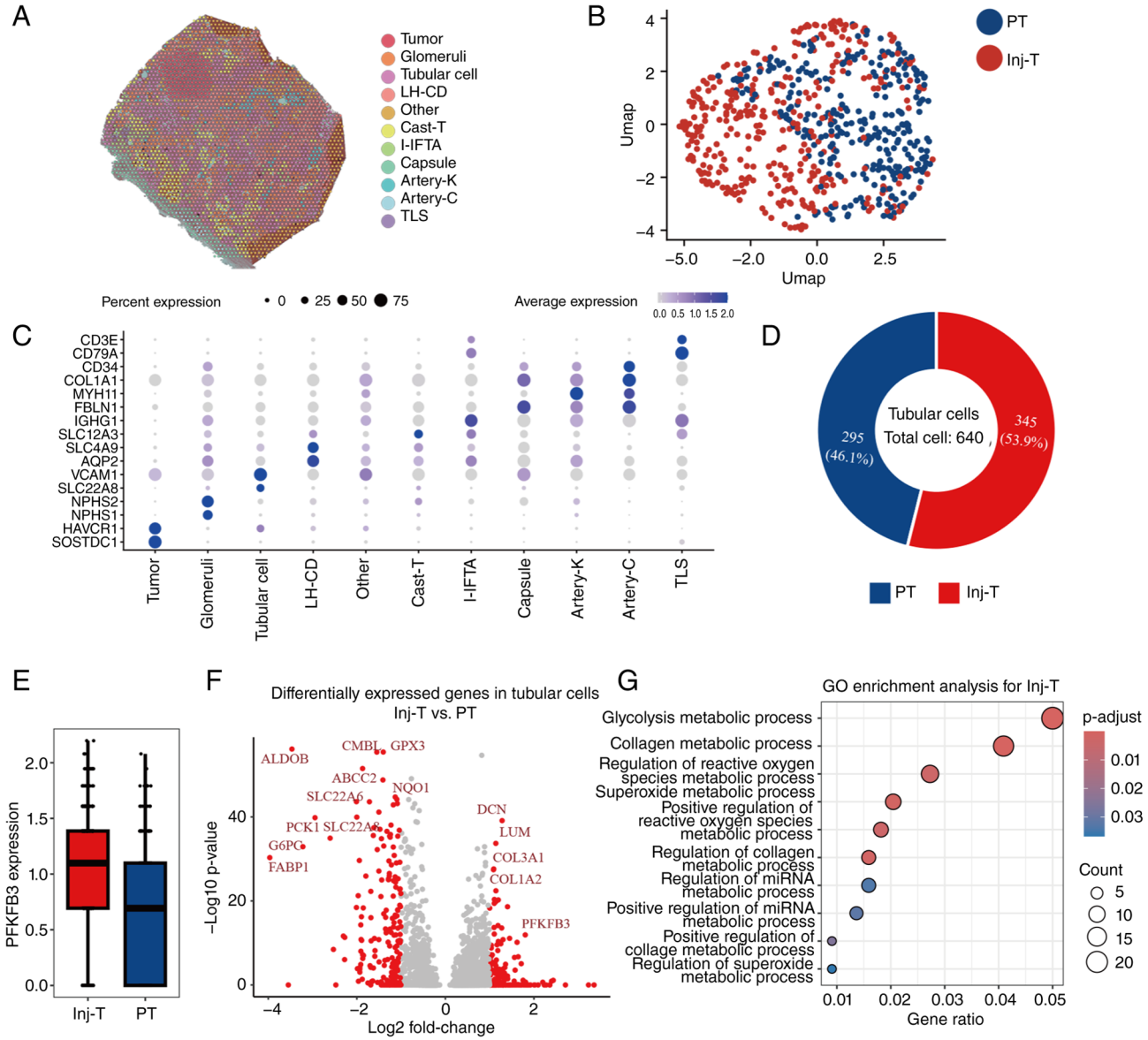

Figure 1. Glycolysis pathway is activated in injury renal tubular cells in DKD. (A and C) Spatial distribution and UMAP analysis of clusters derived from pathological classification. (B and D) Proportion of the PT subclusters and injury PT on the kidney section of DKD patients. (E and F) Expression of PFKFB3 between PT and injury PT subclusters. (G) (GO-BP) enrichment analysis of subcluster-specific genes in injured PT cells. UMAP, Uniform Manifold Approximation and Projection; PT, proximal tubules; DKD, diabetic kidney disease; PFKFB3, 6-phosphofructo-2-kinase/fructose-2,6-biphosphatase 3; GO-BP, Gene Ontology Biological Process.

enrichment of canonical marker genes corresponding to specific renal structures (Fig. 1C). Further subclustering revealed that proximal tubular (PT) cells were divided into normal and injury-associated subtypes, the latter representing 53.9% of the total tubular cells (Fig. 1B and D). The expression levels of PFKFB3 in injured PT cells were markedly increased (Fig. 1E and F). GO enrichment analysis demonstrated that the injury-associated PT cluster was markedly enriched for glycolysis-related pathways, suggesting a metabolic shift contributing to DKD progression (Fig. 1G).

To further determine whether PFKFB3 expression is increased in renal tubules during DKD, its transcript and protein levels were assessed in db/db mice. RT-qPCR revealed a marked elevation of PFKFB3 mRNA levels in kidney derived from db/db mice, compared with those derived from db/m group (Fig. 2A). As shown in Fig. 2B, downregulation of E-cadherin expression, a TEC specific marker critical for maintaining epithelial integrity, together with elevated PFKFB3 expression, indicated that PFKFB3 was actively involved in tubular injury during DKD. In line with the aforementioned results, western blot and IHC analyses confirmed a significant elevation of PFKFB3 protein expression in the db/db group (Fig. 2C-E).

Upregulation of PFKFB3 expression is involved in the development of renal fibrosis in DKD. A kidney-specific PFKFB3 knockdown model was generated via *in situ* renal delivery of AAV9-shRNA to db/db mice to assess the role of PFKFB3 in DKD (Fig. 3A). Silencing of PFKFB3 expression markedly reduced blood glucose levels, serum creatinine and urinary albumin-to-creatinine ratio (UACR) at 20 weeks compared with those noted in the db/db group (Fig. S1A and B; Fig. 3B).

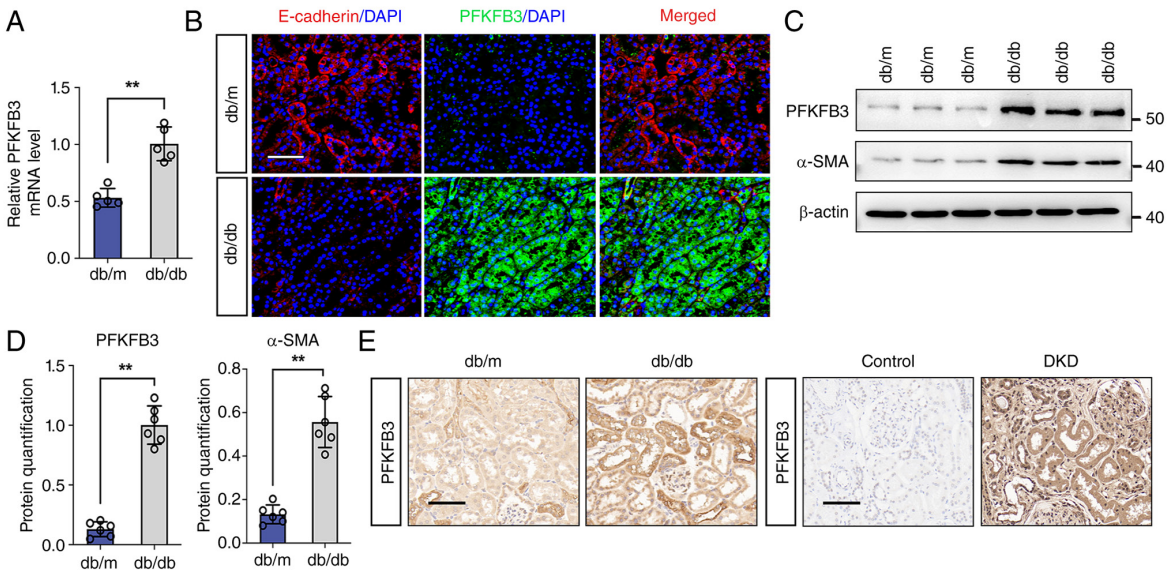

Figure 2. PFKFB3 expression is increased in renal tubular cells in DKD. (A) RT-qPCR for renal PFKFB3 and HK2 in db/m and db/db groups (n=5). (B) Immunostained E-cadherin (red) and PFKFB3 (green), and counterstained with DAPI (blue) by IF staining in db/m and db/db groups (n=6). Scale bar, 50 μm. Protein levels of α-SMA and PFKFB3 in db/m and db/db groups by (C) western blotting and (D) its semi-quantitative analysis (n=6). (E) Representative images of IHC staining for PFKFB3 (scale bar, 50 μm) in db/m and db/db groups or in Control and DKD group (n=6). **P<0.01 vs. db/m group by Student's t-test. PFKFB3, 6-phosphofructo-2-kinase/fructose-2,6-biphosphatase 3; DKD, diabetic kidney disease; RT-qPCR, reverse transcription-quantitative PCR; IF, immunofluorescence; α-SMA, α-smooth muscle actin; IHC, immunohistochemistry.

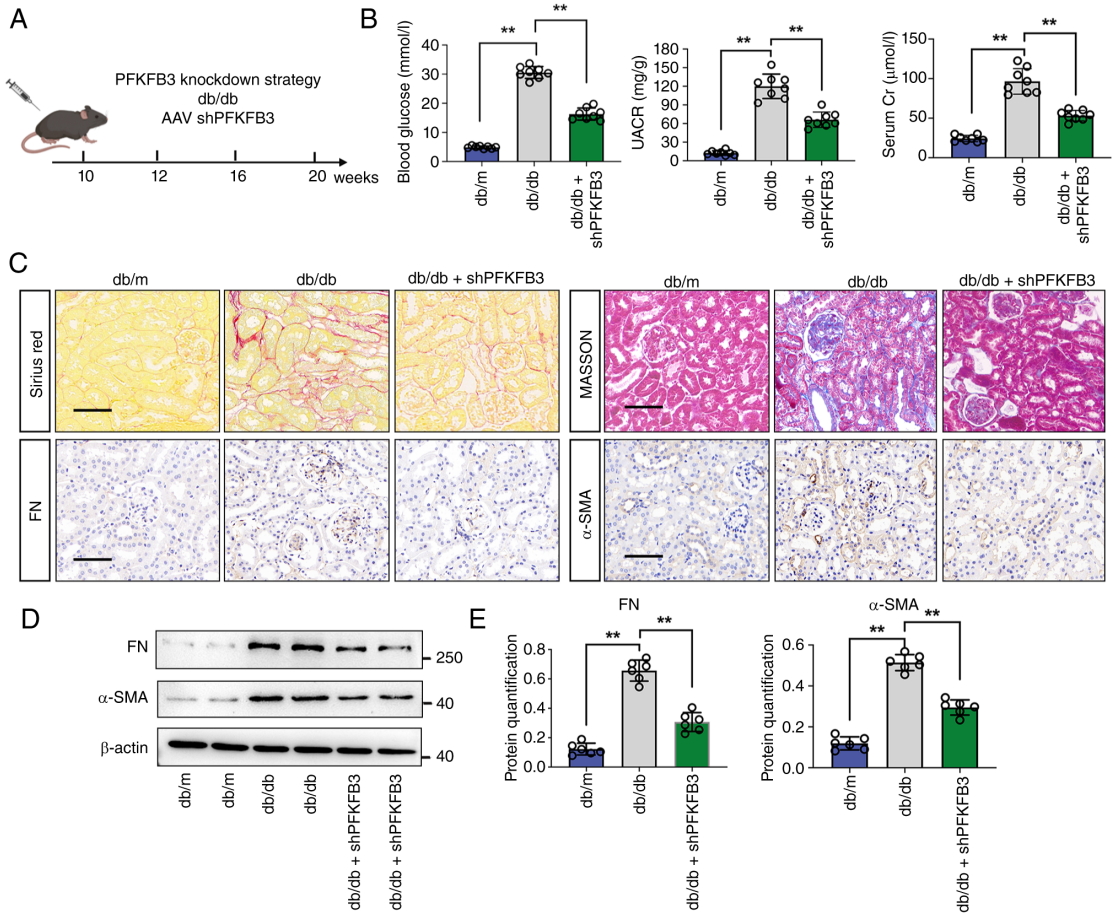

Figure 3. Knockdown of PFKFB3 ameliorates renal fibrosis in db/db mice. (A) Schematic illustration of AAV9-shPFKFB3 injection in the db/db group; (B). Blood glucose levels, UACR and Cr levels in db/m, db/db, and db/db + shPFKFB3 group (n=8). (C) Representative images of Masson, Sirius red staining and IHC staining (α-SMA and FN level) (scale bar=50 μm) in db/m, db/db, and db/db + shPFKFB3 groups (n=6). (D and E) Protein levels of α-SMA and FN in db/m, db/db, and db/db + shPFKFB3 groups by western blotting, with semi-quantitative analyses (n=6). Data represent the mean ± SD from three independent experiments. **P<0.01 vs. db/db group by one-way ANOVA. PFKFB3, 6-phosphofructo-2-kinase/fructose-2,6-biphosphatase 3; AAV, adeno-associated virus; sh, short hairpin; UACR, urinary albumin creatinine ratio; Cr, creatinine; IHC, immunohistochemistry; α-SMA, α-smooth muscle actin; FN, fibronectin.

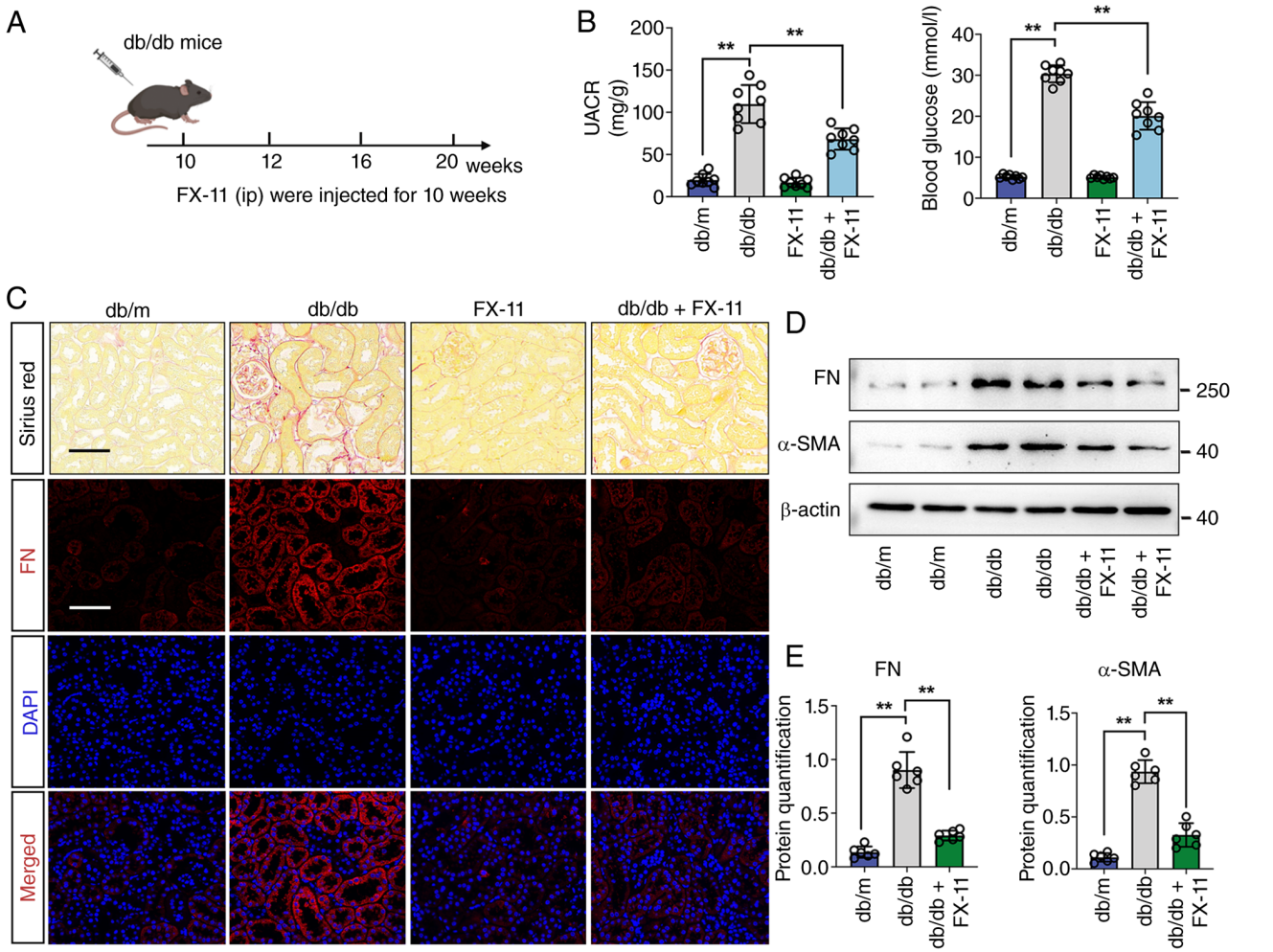

Figure 4. Inhibition of lactate attenuates renal fibrosis in db/db mice. (A) Illustrative overview of the FX-11 intervention strategy in db/db mice. (B) Blood glucose levels and UACR levels in db/m, db/db, db/m + FX-11 and db/db + FX-11 group (n=8). (C) Representative images of Sirius red and IF staining of FN (green), DAPI (blue) in db/m, db/db, db/m + FX-11 and db/db + FX-11 group (n=6). (D and E) Protein levels of α-SMA and FN in db/m, db/db, db/m + FX-11 and db/db + FX-11 groups by western blotting (n=6). Data represent the mean ± SD from three independent experiments. **P<0.01 vs. db/db group by one-way ANOVA. UACR, urinary albumin creatinine ratio; IF, immunofluorescence; FN, fibronectin; α-SMA, α-smooth muscle actin.

Histological examination revealed significant renal fibrosis in db/db mice relative to the db/m group, which was effectively mitigated by shPFKFB3, as demonstrated by Masson's trichrome and Sirius Red staining (Fig. 3C). IHC staining further demonstrated a marked upregulation of fibronectin (FN) and α-SMA expression in the db/db mice, while these elevations were apparently reversed following knockdown of PFKFB3 expression (Fig. 3C). In line with these results, western blot analysis verified that the expression levels of FN and α-SMA were increased in db/db mice compared with those of the db/m mice, and were markedly reduced in the shPFKFB3-treated group (Fig. 3D and E). Conversely, PFKFB3 overexpression in db/db mice exacerbated renal fibrosis (Figs. S1, S2A and S2B). Increased extracellular matrix accumulation and interstitial expansion were observed in these mice, accompanied by upregulation of the expression levels of FN and α-SMA (Fig. S2B-D). Collectively, these results indicated that inhibition of PFKFB3 expression effectively attenuates fibrotic progression in DKD.

PFKFB3-mediated lactate accumulation contributes to the progression of renal fibrosis in DKD. Among all PFKFB isoforms, PFKFB3 exhibits the highest kinase-to-phosphatase activity ratio, which preferentially shunts glucose metabolism toward glycolysis (31,32). Renal lactate levels were initially assessed, revealing a significant increase in db/db mice (Fig. S3). Inhibition of PFKFB3 expression markedly decreased lactate production, while its overexpression further elevated renal lactate accumulation compared with that noted in db/db mice. To determine whether lactate reduction could mitigate fibrotic injury, the lactate dehydrogenase inhibitor FX-11 was administered to db/db mice (Fig. 4A). Treatment with FX-11 led to a substantial decline in blood glucose and UACR (Fig. 4B). Histological evaluation revealed that FX-11 markedly alleviated tubulointerstitial fibrosis, as demonstrated by Sirius Red staining (Fig. 4C). Moreover, FX-11 treatment markedly decreased FN expression in db/db mice, while IF analysis revealed lack of notable changes in the db/m group (Fig. 4C). Consistently, western blot assays confirmed that FX-11 substantially suppressed the protein levels of FN and α-SMA compared with those of db/db group (Fig. 4D and E). Collectively, these findings suggested that lactate accumulation contributes to the progression of renal fibrosis in DKD and that inhibiting lactate production confers a protective effect against renal injury.

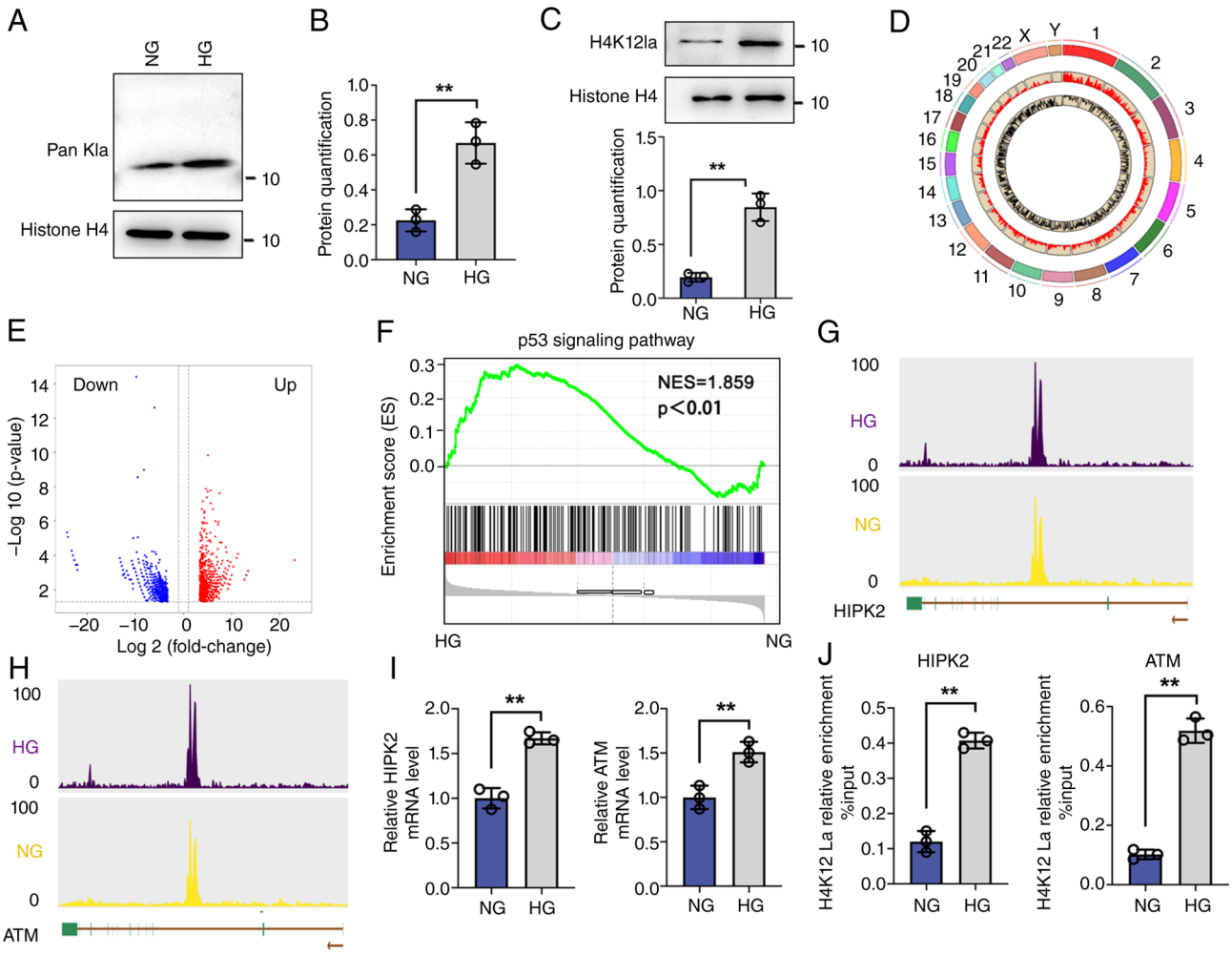

Figure 5. H4K12la initiates p53 pathway related genes under HG condition in HK-2 cells. (A and B) Protein levels of Pan Kla in NG and HG groups by western blotting, and its semi-quantitative analysis (n=3). (C) The protein levels of H4K12la by western blotting in NG and HG groups and their semi-quantitative analyses (n=3); (D and E) Distribution of different genomic distribution of H4K12la peaks between NG and HG group by CUT&Tag. (F) GSEA on the regulation of p53 signaling pathway. (G and H) IGV tracks for HIPK2 and ATM from CUT&Tag analysis. (I) The mRNA level of HIPK2 and ATM in the NG and HG group in HK-2 cells by RT-qPCR (n=3). (J) H4K12la occupancy analysis of HIPK2 and ATM in the NG and HG group in HK-2 cells by CUT&Tag-qPCR (n=3). Data represent the mean ± SD from three independent experiments. **P<0.01 vs. NG group by Student's t-test. HG, high glucose; NG, normal glucose; GSEA, gene set enrichment analysis; RT-qPCR, reverse transcription-quantitative PCR.

Identification of potential downstream genes regulated by of H4K12la. Given that lactate acts as a crucial metabolic substrate facilitating histone lactylation (33,34), it was hypothesized that this epigenetic modification may be aberrantly elevated in the kidneys of the DKD mouse models. Western blot analysis indicated that global histone lactylation was notably increased in TEC following stimulation with HG conditions compared with those noted under NG conditions, with a distinct band at ~11 kDa likely corresponding to histone H4 (Fig. 5A and B). Subsequent immunoblotting further verified that H4K12la levels were markedly upregulated in HG-exposed TECs relative to the NG group (Fig. 5C). Collectively, these data suggested that lactate accumulation promoted H4K12 lactylation under diabetic conditions. To characterize the potential downstream targets of histone lactylation in DKD, CUT&Tag sequencing was conducted using an anti-H4K12la antibody in TECs cultured under NG or HG conditions. HG exposure induced a notable increase in H4K12la enrichment peaks across the genome (Fig. 5D and E). Functional annotation of these peaks revealed a strong positive association with the p53 signaling pathway (Fig. 5F). Integrative analysis identified HIPK2 and ATM as putative lactylation-regulated genes, with genome browser tracks revealing prominent H4K12la enrichment within their respective promoter regions (Fig. 5G and H). RT-qPCR and ChIP-qPCR were performed to confirm the CUT&Tag target genes, revealing their elevated expression, H4K12la enrichment was performed at the promoters of HIPK2 and ATM, with both genes exhibiting substantial H4K12la modification (Fig. 5I and J).

Lactate accumulation is induced by PFKFB3 and facilitates H4K12 histone lactylation in DKD. To elucidate the role of PFKFB3/H4K12la in TEC function during DKD, renal histone lactylation levels were initially assessed. Western blot analysis revealed that inhibition of PFKFB3 expression markedly decreased global histone lactylation in db/db mice (Fig. S4A and B; Fig. 6A and B). Knockdown of PFKFB3 expression in HK-2 cells led to reduced histone lactylation (Fig. 6C and D). Immunofluorescence co-staining of H4K12la (red) and E-cadherin (green) demonstrated markedly elevated H4K12la

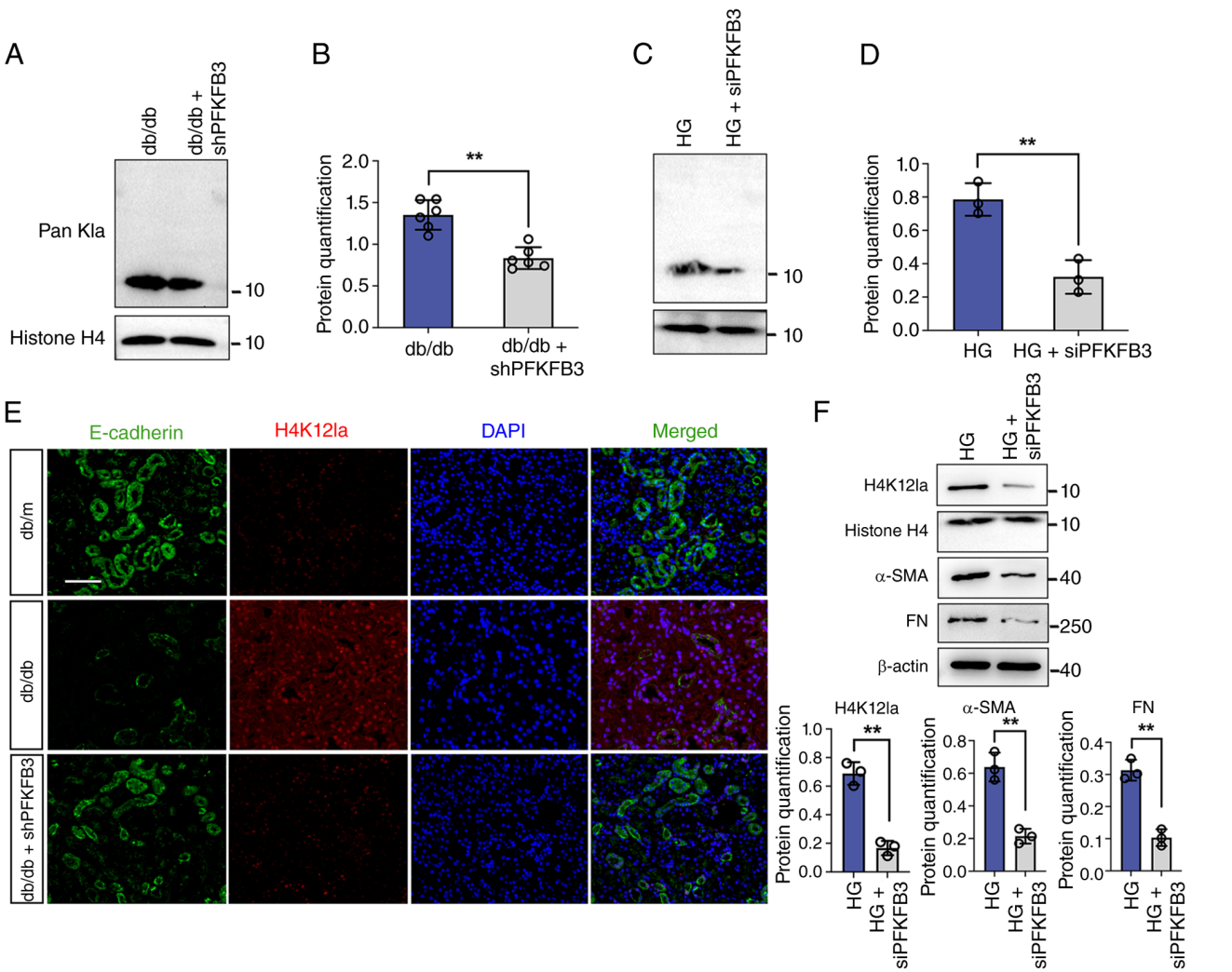

Figure 6. PFKFB3-driven lactate triggers H4K12 lactylation in DKD. (A and B) Protein levels of Pan Kla in db/db and db/db + shPFKFB3 groups by western blotting and its semi-quantitative analysis (n=6). (C and D) Protein levels of Pan Kla in HG and HG + siPFKFB3 groups by western blotting and its semi-quantitative analysis (n=3). (E) Immunostained E-cadherin (green) and H4K12la (red), and counterstained with DAPI (blue) by IF staining in db/m, db/db and db/db + shPFKFB3 groups (n=6). Scale bar, 50 μm. (F) The protein levels of H4K12la, α-SMA and FN by western blot in HG and HG + siPFKFB3 groups, and their semi-quantitative analyses (n=3). Data represent the mean ± SD from three independent experiments. **P<0.01 vs. (D and F) HG group or (B) db/db group by Student's t-test. PFKFB3, 6-phosphofructo-2-kinase/fructose-2,6-biphosphatase 3; DKD, diabetic kidney disease; sh, short hairpin; HG, high glucose; si, small interfering; IF, immunofluorescence; FN, fibronectin.

signals in the renal tubules of db/db mice, which were attenuated by inhibition of PFKFB3 expression (Fig. 6E). Moreover, transfection of HK-2 cells with small interfering (si)PFKFB3 suppressed the expression levels of H4K12la, α-SMA and FN (Fig. 6F). Extracellular flux analysis revealed that PFKFB3 silencing reduced glycolytic capacity and lactate accumulation compared with those noted in HG group (Fig. 7A and B). In HK-2 cells, treatment with siPFKFB3 led to a decrease in the expression levels of H4K12la, HIPK2, α-smooth muscle actin (α-SMA), and FN compared with those noted in the HG group. Notably, excess lactate production reversed this suppression, exacerbating fibrotic responses and increasing H4K12la and HIPK2 levels relative to siPFKFB3-treated cells (Fig. 7C and D). Double immunofluorescence staining further validated the lactate-induced alterations in the levels of H4K12la and HIPK2 in HK-2 cells (Fig. 7E). Collectively, these results indicated that PFKFB3-driven lactate accumulation promotes tubular fibrosis through H4K12la-mediated regulation of profibrotic signaling.

Discussion

Despite remarkable progress in elucidating the pathogenesis and diagnostic markers of DKD, this disease is associated with major complications contributing to morbidity in diabetic patients (35-37). Growing evidence indicates that metabolic reprogramming in renal tubules is a key driver of fibrotic progression in DKD (5,38). In particular, enhanced glycolytic flux and elevated lactate accumulation have been consistently observed in both diabetic kidneys and in the circulation (23,39,40). A marked expression of PFKFB3 was observed, mainly in TECs derived from patients with DKD and mouse models; the results verified that silencing of PFKFB3 expression could markedly alleviate renal fibrosis. With regard to its mechanism of action, deficiency of PFKFB3 expression inhibited H4K12 lactylation and transcriptional activation of HIPK2. Collectively, the findings reveal that tubular PFKFB3-driven glycolytic activation promotes renal fibrosis via lactate-dependent epigenetic regulation of HIPK2.

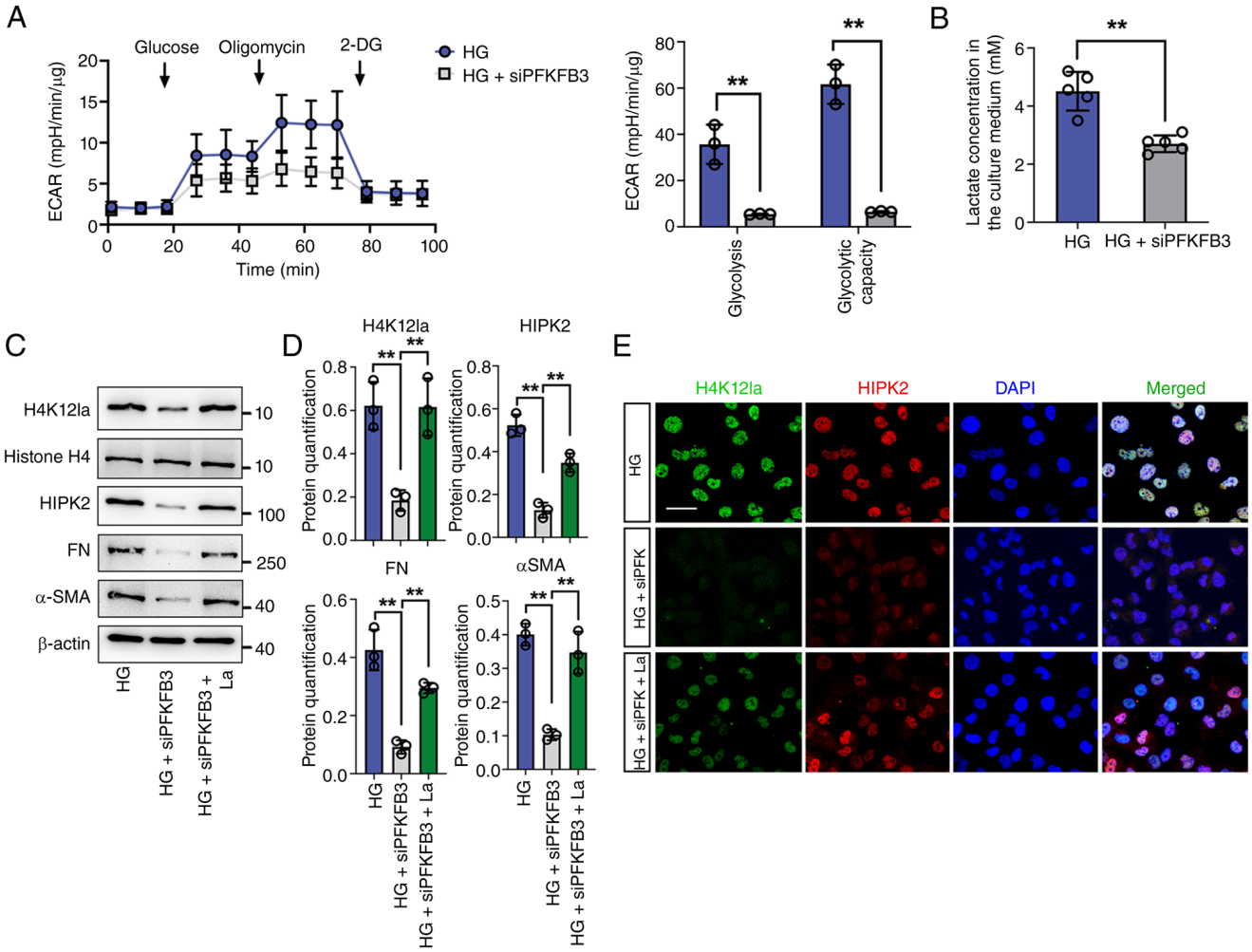

Figure 7. PFKFB3-mediated H4K12la initiates renal tubule fibrosis in DKD. (A) The ECAR levels after culturing with glucose followed by oligomycin and 2-DG in HG and HG + siPFKFB3 groups (n=3). (B) The lactate concentration in HK-2 cells in the HG and HG + siPFKFB3 groups (n=5). (C and D) Protein levels of H4K12la, HIPK2, FN and α-SMA in HG, HG + siPFKFB3 and HG + siPFKFB3 + La groups in HK-2 cells by western blotting, with semi-quantitative analyses (n=3). (E) Immunostaining for H4K12la (green) and HIPK2 (red), counterstained with DAPI (blue) in HG, HG + siPFKFB3 and HG + siPFKFB3 + La (scale bar, 50 μm). Data represent the mean ± SD from three independent experiments. **P<0.01 versus HG group (A and B) by Student's t-test or HG + siPFKFB3 group (D) by one-way ANOVA. PFKFB3, 6-phosphofructo-2-kinase/fructose-2,6-biphosphatase 3; DKD, diabetic kidney disease; ECAR, extracellular acidification rate; HG, high glucose; si, small interfering; FN, fibronectin; α-SMA, α-smooth muscle actin.

The PFKFB family of enzymes plays a pivotal role in regulating glycolytic flux. Among its isoforms, PFKFB3 possesses the highest kinase-to-phosphatase activity ratio, thereby preferentially directing glucose toward glycolysis (41,42). Its catalytic product, fructose-2,6-bisphosphate, activates phosphofructokinase 1 and regulates diverse cellular processes including differentiation (43) and inflammation (44). Under hypoxic conditions, glycolysis is typically enhanced and the preservation of renal structure and function relies heavily on the maintenance of balanced energy metabolism (45). Previous studies have reported that diabetic kidneys display fibrotic alterations associated with aberrant glycolytic activation (45,20,21). In endothelial cells, PFKFB3-driven glycolysis enhances metabolic flux and promotes the production of metabolites, thereby exacerbating renal inflammation (46). Similarly, PFKFB3-mediated glycolytic upregulation promotes lactate accumulation, triggers osteogenic trans-differentiation of vascular smooth muscle cells and accelerates vascular calcification in chronic kidney disease models (47). Collectively, these findings indicate that dysregulated glycolysis contributes to the pathogenesis of renal fibrogenesis. In the present study, a significant upregulation in the expression of PFKFB3 was noted in kidneys from patients with DKD and in diabetic mice. Genetic suppression of PFKFB3 mitigated glycolytic activation and ameliorated renal injury. These results suggested that excessive PFKFB3-driven glycolysis plays a causal role in promoting renal fibrosis in DKD.

Elevated glycolytic flux is known to drive excessive lactate accumulation. In addition to serving as a metabolic byproduct, lactate acts as a pivotal signaling intermediate that modulates immune responses and remodels tissue microenvironments via its influence on cellular signaling and transcriptional regulation (20,48,49). In diabetic kidneys, metabolic reprogramming is characterized by increased lactate dehydrogenase A (LDHA) expression and lactate accumulation, accompanied by reduced ATP generation. Pharmacological inhibition of LDHA effectively decreases lactate levels, restores renal energy homeostasis and mitigates both structural renal damage and albuminuria (40). Clinical and experimental data further reveal a close correlation between circulating glucose

and lactate levels in circulation and in urine of diabetic individuals. Proximal tubular epithelial cells represent a major source of this lactate production, which can be suppressed by sodium-glucose cotransporter-2 (23). These findings collectively implicate lactate accumulation as a key pathogenic contributor to the onset and progression of DKD and its reduction confers reno-protective effects by limiting fibrotic remodeling. Lactate-triggered histone lactylation, an emerging epigenetic modification, acts as a vital molecular bridge connecting lactate metabolism with gene regulatory networks via modulating lactate generation, distribution and utilization. This epigenetic modification induces conformational remodeling of histone proteins, affects chromatin accessibility and modulates transcription, with its levels directly governed by lactate spatial distribution, therefore linking cellular metabolism to epigenetic control of gene expression (50-52). Notably, H4K12 lactylation was markedly elevated in diabetic kidneys and in *in vitro* models in a lactate-dependent manner. CUT&Tag profiling further identified prominent H4K12la enrichment at the HIPK2 promoter region, promoting its transcriptional activation and amplifying downstream glycolytic signaling. Nevertheless, the mechanistic crosstalk between the pathogenesis of DKD and HIPK2 activation remains incompletely elucidated.

While the present study elucidated the role of HIPK2 H4K12 lactylation in regulating glycolysis *in vivo* and *in vitro*, several limitations should be considered. First, the potential crosstalk between histone lactylation and other post-translational modifications, such as acetylation remains unresolved. Histone modifications are dynamically governed by enzymes responsible for the addition, removal and recognition of specific markers. A previous study indicated that histone lactylation is highly reliant on the intracellular level of lactyl-CoA and the enzymatic activity of acyltransferases including P300/CBP, which function as major mediators of histone lactylation modification in macrophages (53). Conversely, deacetylases including histone deacetylase 1-3 and members of the Sirtuin family can also catalyze the removal of lactyl groups from histone lysines, exerting de-lactylation activity (54,55). In the present study, the contribution of the histone-modifying enzymes to lactylation within TECs during DKD was not investigated. Further studies employing quantitative mass spectrometry and site-directed mutagenesis are warranted to determine the specific enzymes and residues mediating histone lactylation and to elucidate its biological implications in renal pathology.

Collectively, the findings of the present study revealed that PFKFB3-dependent lactate production modulates gene transcription via histone lactylation. It was further demonstrated that the upregulation of PFKFB3 expression in tubular epithelial cells under diabetic kidney disease conditions is essential for the progression of renal fibrosis and that histone lactylation acting downstream of PFKFB3 serves as a key determinant of downstream gene expression. Therefore, these findings suggest that maintaining metabolic stability via epigenetic regulation in tubular cells during injury could be an effective strategy for delaying DKD development.

Acknowledgements

Not applicable.

Funding

The present study was supported in part by the Guangdong Natural Science Foundation General Program (grant no. 2025A1515010621), in part by Guangdong Medical University Clinical and Basic Science Innovation Special Project (grant nos. GDMULCJC2024047 and GDMULCJC2024086), in part by Hundreds Youth Research Projects of Guangdong Medical University (grant no. GDMUD2024011) and in part by Medical Science and Technology Research Foundation of Guangdong Province (grant no. B2025045).

Availability of data and materials

The data generated in the present study may be requested from the corresponding author.

Authors' contributions

LX conceived and designed the experiments. FX contributed to clinical study design and collected the data. MX drafted the manuscript. LF and YZ conceived the study. HW and XG performed the data analysis. LX revised the manuscript. FX and LF performed the functional experiments. SG contributed to data acquisition and critically revised the manuscript. All data were produced by the authors without the use of a paper mill. The authors collectively accept responsibility for the accuracy and integrity of the work. LX and FX confirm the authenticity of all the raw data. All authors read and approved the final manuscript.

Ethics approval and consent to participate

All animal studies were approved by the Ethics Committee on the Care and Use of Laboratory Animals of Guangdong Medical University (approval no. GDY2402166).

Patient consent for publication

Not applicable.

Competing interests

The authors declare that they have no competing interests.

References

1. Pavkov ME and Miyamoto Y: Diabetes and kidney disease. IDF Diabetes Atlas 2023. https://diabetesatlas.org/resources/idf-diabetes-atlas-reports/diabetes-and-kidney-disease/. Accessed Nov 12, 2025.
2. Martinez Leon V, Hilburg R and Susztak K: Mechanisms of diabetic kidney disease and established and emerging treatments. Nat Rev Endocrinol 22: 21-35, 2026.
3. Mentz RJ, Anker SD, Pitt B, Rossing P, Ruilope LM, Gebel M, Kolkhof P, Lawatscheck R, Rohwedder K and Bakris GL; on behalf of the FIDELIO-DKD and FIGARO-DKD investigators: Efficacy and safety of finerenone in patients with chronic kidney disease and type 2 diabetes by diuretic use: A FIDELITY analysis. Eur J Heart Fail 27: 764-774, 2025.
4. Zhao H and Guo J: Macrophages in focus: Key drivers and therapeutic opportunities in diabetic kidney disease. Int J Biol Sci 21: 4647-4662, 2025.

5. Naaman SC and Bakris GL: Diabetic nephropathy: Update on pillars of therapy slowing progression. Diabetes Care 46: 1574-1586, 2023.
6. Mimura I, Chen Z and Natarajan R: Epigenetic alterations and memory: Key players in the development/progression of chronic kidney disease promoted by acute kidney injury and diabetes. Kidney Int 107: 434-456, 2025.
7. Mohandes S, Doke T, Hu H, Mukhi D, Dhillon P and Susztak K: Molecular pathways that drive diabetic kidney disease. J Clin Invest 133: e165654, 2023.
8. Fan X, Yang M, Lang Y, Lu S, Kong Z, Gao Y, Shen N, Zhang D and Lv Z: Mitochondrial metabolic reprogramming in diabetic kidney disease. Cell Death Dis 15: 442, 2024.
9. Hong Q, Kim H, Cai GY, Chen XM, He JC and Lee K: Modulation of TGF-β signaling new approaches toward kidney disease and fibrosis therapy. Int J Biol Sci 21: 1649-1665, 2025.
10. Zou Y, Yiu WH, Lok SWY, Ma J, Feng Y, Lai KN and Tang SCW: Tubular FoxP2 and kidney fibrosis. J Am Soc Nephrol 36: 544-558, 2025.
11. Saraswati S, Martínez P, Serrano R, Mejías D, Graña-Castro O, Díaz RÁ, Flores JM and Blasco MA: Telomere dysfunction in renal tubular epithelial cells leads to kidney fibrosis. J Am Soc Nephrol 36: 2348-2363, 2025.
12. Yao L, Liang X, Liu Y, Li B, Hong M, Wang X, Chen B, Liu Z and Wang P: Non-steroidal mineralocorticoid receptor antagonist finerenone ameliorates mitochondrial dysfunction via PI3K/Akt/eNOS signaling pathway in diabetic tubulopathy. Redox Biol 68: 102946, 2023.
13. Wang M, Li Q, Wang S, Zuo L, Hai Y, Yuan S, Li X, Huang X, Yang C, Yao L, *et al*: Astragaloside IV protects renal tubular epithelial cells against oxidative stress-induced injury by upregulating CPT1A-mediated HSD17B10 lysine succinylation in diabetic kidney disease. Phytother Res 38: 4519-4540, 2024.
14. Wu YW, Chen JW, Lin LY, Huang JH, Chang CC and Chang TT: FABP4 inhibition protects renal tubular cells and ameliorates renal inflammation in diabetic kidney disease. Biochem Pharmacol 236: 116899, 2025.
15. Hommos MS, Glassock RJ and Rule AD: Structural and functional changes in human kidneys with healthy aging. J Am Soc Nephrol 28: 2838-2844, 2017.
16. Bao Y, Shan Q, Lu K, Yang Q, Liang Y, Kuang H, Wang L, Hao M, Peng M, Zhang S and Cao G: Renal tubular epithelial cell quality control mechanisms as therapeutic targets in renal fibrosis. J Pharm Anal 14: 100933, 2024.
17. Liu X, Zhang Y, Wang Y, Yang Y, Qiao Z, Zhan P, Jin H, Xu Q, Tang W, Sun Y, *et al*: Tubular MYDGF slows progression of chronic kidney disease by maintaining mitochondrial homeostasis. Adv Sci (Weinh) 12: e2409756, 2025.
18. Huang H, Han Y, Zhang Y, Zeng J, He X, Cheng J, Wang S, Xiong Y, Yin H, Yuan Q, *et al*: Deletion of pyruvate carboxylase in tubular epithelial cell promotes renal fibrosis by regulating SQOR/cGAS/STING-mediated glycolysis. Adv Sci (Weinh) 12: e2408753, 2025.
19. Nishima N and Tanaka S: Lactate: A missing link between metabolism and inflammation in CKD progression? Kidney Int 106: 183-185, 2024.
20. Zhu W, Guo S, Sun J, Zhao Y and Liu C: Lactate and lactylation in cardiovascular diseases: Current progress and future perspectives. Metabolism 158: 155957, 2024.
21. Xie W, He Q, Zhang Y, Xu X, Wen P, Cao H, Zhou Y, Luo J, Yang J and Jiang L: Pyruvate kinase M2 regulates mitochondrial homeostasis in cisplatin-induced acute kidney injury. Cell Death Dis 14: 663, 2023.
22. Shao M, Chen D, Wang Q, Guo F, Wei F, Zhang W, Gan T, Luo Y, Fan X, Du P, *et al*: Canagliflozin regulates metabolic reprogramming in diabetic kidney disease by inducing fasting-like and aestivation-like metabolic patterns. Diabetologia 67: 738-754, 2024.
23. Darshi M, Kugathasan L, Maity S, Sridhar VS, Fernandez R, Limonte CP, Grajeda BI, Saliba A, Zhang G, Drel VR, *et al*: Glycolytic lactate in diabetic kidney disease. JCI Insight 9: e168825, 2024.
24. Ye Z, Sun Y, Yang S, Li L, Li B, Xia Y, Yuan T, Yu W, Chen L, Zhou X and Cheng F: Lgals3 promotes calcium oxalate crystal formation and kidney injury through histone lactylation-mediated FGFR4 activation. Adv Sci (Weinh) 12: e2413937, 2025.
25. Xiang T, Wang X, Huang S, Zhou K, Fei S, Zhou B, Yue K, Li Q, Xue S, Dai Y, *et al:* Inhibition of PKM2 by shikonin impedes TGF-β1 expression by repressing histone lactylation to alleviate renal fibrosis. Phytomedicine 136: 156324, 2025.
26. Zhang X, Chen J, Lin R, Huang Y, Wang Z, Xu S, Wang L, Chen F, Zhang J, Pan K and Yin Z: Lactate drives epithelial-mesenchymal transition in diabetic kidney disease via the H3K14la/KLF5 pathway. Redox Biol 75: 103246, 2024.
27. Arat S, Huynh R, Kumpf S, Qian J, Shoieb A, Virgen-Slane R, Voigt F, Xie Z and Jakubczak JL: Effects of donor source on transcriptomic profiles of human kidney tissue. FASEB J 37: e22804, 2023.
28. Mei H, Jing T, Liu H, Liu Y, Zhu X, Wang J and Xu L: Ursolic acid alleviates mitotic catastrophe in podocyte by inhibiting autophagic P62 accumulation in diabetic nephropathy. Int J Biol Sci 20: 3317-3333, 2024.
29. Leary S, Underwood W, Anthony R, Cartner S, Grandin T, Greenacre C, Gwaltney-Brant S, McCrackin MA, Meyer R, Miller D, *et al*: AVMA Guidelines for the Euthanasia of Animals: 2020 Edition. American Veterinary Medical Association, Schaumburg, IL, 2020.
30. Livak KJ and Schmittgen TD: Analysis of relative gene expression data using real-time quantitative PCR and the 2(-delta delta C(T)) method. Methods 25: 402-408, 2001.
31. Lin XF, Cui XN, Yang J, Jiang YF, Wei TJ, Xia L, Liao XY, Li F, Wang DD, Li J, *et al*: SGLT2 inhibitors ameliorate NAFLD in mice via downregulating PFKFB3, suppressing glycolysis and modulating macrophage polarization. Acta Pharmacol Sin 45: 2579-2597, 2024.
32. Zhong YX, Zhao HB, Lian MH, Shen JM, Li CX, Ma HM, Xu D, Chen GQ and Zhang C: SUMOylated hnRNPM suppresses PFKFB3 phosphorylation to regulate glycolysis and tumorigenesis. Cancer Lett 616: 217573, 2025.
33. Li Z, Liang Z, Qi H, Luo X, Wang M, Du Z and Guo W: Lactate shuttling links histone lactylation to adult hippocampal neurogenesis in mice. Dev Cell 60: 1182-1198.e8, 2025.
34. Zhang J, Wu D, Zeng F, Gu H, Li C, Cata JP, Guo K, Miao C and Zhang H: Lactate metabolic reprogramming and histone lactylation modification in sepsis. Int J Biol Sci 21: 5034-5055, 2025.
35. Jung CY and Yoo TH: Pathophysiologic mechanisms and potential biomarkers in diabetic kidney disease. Diabetes Metab J 46: 181-197, 2022.
36. Das S, Devi Rajeswari V, Venkatraman G, Elumalai R, Dhanasekaran S and Ramanathan G: Current updates on metabolites and its interlinked pathways as biomarkers for diabetic kidney disease: A systematic review. Transl Res 265: 71-87, 2024.
37. Yang H, Sun J, Sun A, Wei Y, Xie W, Xie P, Zhang L, Zhao L and Huang Y: Podocyte programmed cell death in diabetic kidney disease: Molecular mechanisms and therapeutic prospects. Biomed Pharmacother 177: 117140, 2024.
38. Hu H, Li W, Hao Y, Peng Z, Zou Z and Liang W: Baicalin ameliorates renal fibrosis by upregulating CPT1α-mediated fatty acid oxidation in diabetic kidney disease. Phytomedicine 122: 155162, 2024.
39. Yang G, Liu X, Li Y, Li L, Xiang J, Liang Z, Jiang M and Yang S: TRIM65 as a key regulator of ferroptosis and glycolysis in lactate-driven renal tubular injury and diabetic kidney disease. Cell Rep 44: 116091, 2025.
40. Azushima K, Kovalik JP, Yamaji T, Ching J, Chng TW, Guo J, Liu JJ, Nguyen M, Sakban RB, George SE, *et al*: Abnormal lactate metabolism is linked to albuminuria and kidney injury in diabetic nephropathy. Kidney Int 104: 1135-1149, 2023.
41. Zeng H, Pan T, Zhan M, Hailiwu R, Liu B, Yang H and Li P: Suppression of PFKFB3-driven glycolysis restrains endothelial-to-mesenchymal transition and fibrotic response. Signal Transduct Target Ther 7: 303, 2022.
42. Bartrons R, Rodríguez-García A, Simon-Molas H, Castaño E, Manzano A and Navarro-Sabaté À: The potential utility of PFKFB3 as a therapeutic target. Expert Opin Ther Targets 22: 659-674, 2018.
43. Ma J, Li X, Li Q, Sun Z, You Y, Zhang L, Ji Z, Zhou H, Zhang Q, Wang L, *et al*: Niacin regulates glucose metabolism and osteogenic differentiation via the SIRT2-C/EBPβ-AREG signaling axis. Biomed Pharmacother 180: 117447, 2024.
44. Wang TT, Han T, Xiao X, Guo D, Sun X, Liu Y, Zhao L, Xu H, Li R, Jiang L, *et al*: SIRT3 deficiency reduces PFKFB3-driven T-cell glycolysis and promotes arthritic inflammation. Sci China Life Sci 68: 1755-1769, 2025.
45. Jiang A, Liu J, Wang Y and Zhang C: cGAS-STING signaling pathway promotes hypoxia-induced renal fibrosis by regulating PFKFB3-mediated glycolysis. Free Radic Biol Med 208: 516-529, 2023.

46. Song C, Wang S, Fu Z, Chi K, Geng X, Liu C, Cai G, Chen X, Wu D and Hong Q: IGFBP5 promotes diabetic kidney disease progression by enhancing PFKFB3-mediated endothelial glycolysis. Cell Death Dis 13: 340, 2022.
47. Li Y, Chen X, Xu X, Chen C, Min M, Liang D, Ren J and Mao H: OTUB2 contributes to vascular calcification in chronic kidney disease via the YAP-mediated transcription of PFKFB3. Theranostics 15: 1185-1204, 2025.
48. Chen J, Huang Z, Chen Y, Tian H, Chai P, Shen Y, Yao Y, Xu S, Ge S and Jia R: Lactate and lactylation in cancer. Signal Transduct Target Ther 10: 38, 2025.
49. Llibre A, Kucuk S, Gope A, Certo M and Mauro C: Lactate: A key regulator of the immune response. Immunity 58: 535-554, 2025.
50. Wang T, Ye Z, Li Z, Jing DS, Fan GX, Liu MQ, Zhuo QF, Ji SR, Yu XJ, Xu XW and Qin Y: Lactate-induced protein lactylation: A bridge between epigenetics and metabolic reprogramming in cancer. Cell Prolif 56: e13478, 2023.
51. Yu X, Yang J, Xu J, Pan H, Wang W, Yu X and Shi S: Histone lactylation: From tumor lactate metabolism to epigenetic regulation. Int J Biol Sci 20: 1833-1854, 2024.
52. Li Y, Cao Q, Hu Y, He B, Cao T, Tang Y, Zhou XP, Lan XP and Liu SQ: Advances in the interaction of glycolytic reprogramming with lactylation. Biomed Pharmacother 177: 116982, 2024.
53. Li F, Si W, Xia L, Yin D, Wei T, Tao M, Cui X, Yang J, Hong T and Wei R: Positive feedback regulation between glycolysis and histone lactylation drives oncogenesis in pancreatic ductal adenocarcinoma. Mol Cancer 23: 90, 2024.
54. Sheng X, Lin H, Cole PA and Zhao Y: Biochemistry and regulation of histone lysine L-lactylation. Nat Rev Mol Cell Biol 27: 95-109, 2025.
55. Liao Z, Chen B, Yang T, Zhang W and Mei Z: Lactylation modification in cardio-cerebral diseases: A state-of-the-art review. Ageing Res Rev 104: 102631, 2025.